Geophysical Research Letters

RESEARCH LETTER
10.1029/2022GL099638

Key Points:

- The kinetic physics in the magnetohydrodynamics with embedded particle-in-cell model plays an important role in reproducing sawtooth oscillations
- Kinetic reconnection in the magnetotail can produce sawtooth-like oscillations without varying ionospheric outflow

Correspondence to:

X. Wang,
xtwang@umich.edu

Citation:

Wang, X., Chen, Y., & Tóth, G. (2022). Simulation of magnetospheric sawtooth oscillations: The role of kinetic reconnection in the magnetotail. *Geophysical Research Letters*, *49*, e2022GL099638. https://doi.org/10.1029/2022GL099638

Received 23 MAY 2022
Accepted 1 AUG 2022

Simulation of Magnetospheric Sawtooth Oscillations: The Role of Kinetic Reconnection in the Magnetotail

Xiantong Wang[1], Yuxi Chen[1,2], and Gábor Tóth[1]

[1]Department of Climate and Space Sciences and Engineering, University of Michigan, Ann Arbor, MI, USA, [2]Now at Princeton Plasma Physics Laboratory, Princeton University, Princeton, NJ, USA

Abstract Magnetospheric sawtooth oscillations are observed during strong and steady solar wind driving conditions. The simulation results of our global magnetohydrodynamics (MHD) model with embedded kinetic physics show that when the total magnetic flux carried by constant solar wind exceeds a threshold, sawtooth-like magnetospheric oscillations are generated. Different from previous works, this result is obtained without involving time-varying ionospheric outflow in the model. The oscillation period and amplitude agree well with observations. The simulated oscillations cover a wide range of local times, although the distribution of magnitude as a function of longitude is different from observations. Our comparative simulations using ideal or Hall MHD models do not produce global time-varying features, which suggests that kinetic reconnection physics in the magnetotail is a major contributing factor to sawtooth oscillations.

Plain Language Summary The magnetospheric sawtooth oscillation is a global-scale phenomenon in the Earth's magnetosphere. Observations and simulations suggest that the oxygen outflow from the ionosphere is inducing the sawtooth oscillations by affecting the rate of the magnetic reconnection: a fundamental physical process converting magnetic energy to plasma energy. We use a model where the magnetic reconnection is solved by kinetic physics and show that sawtooth-like oscillations can be induced if the incoming solar wind magnetic flux exceeds a threshold. This work proposes a new mechanism contributing to magnetospheric sawtooth oscillations.

1. Introduction

More than two decades ago, Belian et al. (1995) observed giant quasi-periodic, global flux variations with periods of 2–4 hr through the Los Alamos National Laboratory energetic particle detectors, Charged Particle Analyzer, and the time variations of electron fluxes at geosynchronous orbit resemble a tooth of a saw blade: a slow decrease followed by a rapid increase (Henderson, 2004). Moreover, this feature is observed in a wide range of magnetic local time (MLT), which distinguishes it from isolated substorms. These periodic injections also have impacts on other geospace features like magnetic field variations at geosynchronous orbit, the auroral electrojet index, and the polar cap index (Cai et al., 2006; Henderson, Reeves, et al., 2006; Henderson, Skoug, et al., 2006; Huang et al., 2003). Although there is still no definitive answer to the mechanisms producing the sawtooth oscillations, numerical simulations for the coupled magnetosphere-ionosphere system have demonstrated a possible explanation related to the O^+ outflow from the ionosphere (Brambles et al., 2011). The basic idea of this theory is that the periodic mass loading and unloading from the ionospheric outflow alters the reconnection rate in the magnetotail current sheet. The different reconnection rate results in different magnetic field configuration in the tail, which modulates the ionospheric outflow rate. This feed back loop produces the periodic oscillations.

There are a number of studies establishing this theory over the past decade. Wiltberger et al. (2010) uses the Multi-Fluid Lyon Fedder Mobarry model to demonstrate that the out-flowing cusp ions transported to the tail can have an effect on the magnetic configuration and trigger substorm dipolarizations. Yu and Ridley (2013) also shows that cusp O^+ outflow can influence the development of isolated substorms. Brambles et al. (2011) applies an empirical power-law relationship between the Alfvénic Poynting flux and the resulting ionospheric outflow flux at the simulation inner boundary and shows that this outflow can induce quasi-periodic substorms resembling observed sawtooth oscillations. In a follow-up study, Ouellette et al. (2013) studies how the ion composition of the plasma sheet and magnetotail affects the tail reconnection rate. They hypothesized that the massive outflow inflates the magnetosphere and enables the development of the next sawtooth oscillation. Later on, Brambles et al. (2013) used the same model on two different types of sawtooth events induced by different

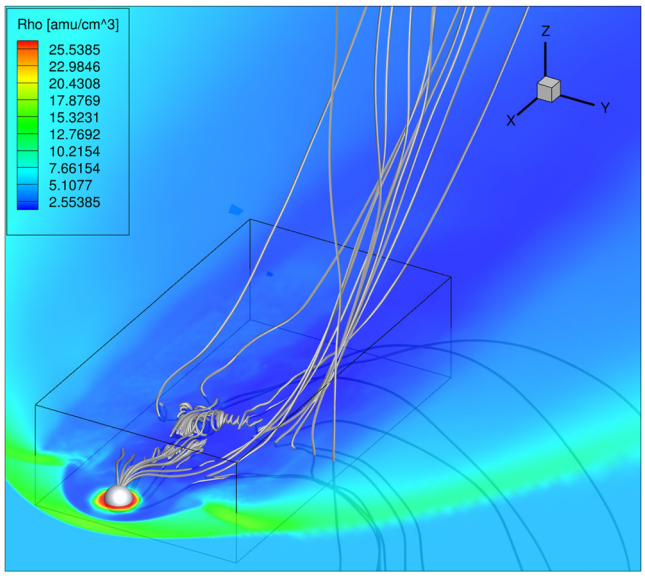

Figure 1. The global structure of Earth's magnetosphere at simulation time $t = 1$ hr from the magnetohydrodynamics with embedded particle-in-cell simulation with the strong solar wind driving condition. The color contour shows the mass density in the equatorial plane. The white spherical surface is the inner boundary at 2.5 R_E. The gray rods are magnetic field lines of two flux ropes in the magnetotail. The black box is the domain of the PIC model that covers potential magnetic reconnection sites in the tail.

external driving conditions: the Stream Interaction Region (SIR)-driven 24 October 2002 event and the Coronal Mass Ejection (CME)-driven 18 April 2002 event. They find that quasi-periodic substorms occurred in the SIR event without outflow while no periodic substorm occurs in the CME event without outflow. Presumably, the quasi-periodic substorms in the SIR event are triggered by the variations in the external driving condition while in the CME event, they are more related to the internal mechanism of the magnetosphere. More recently, Lund et al. (2018) uses mass composition data from the Cluster satellites and discovers the role ionospheric outflow plays in inducing sawtooth oscillations. They find during the CME events, the O^+ in the mid-tail plasma sheet is mostly from the cusp/dayside while the nightside outflow preconditions the plasma sheet to enable the sawtooth oscillations. The recent work by Zhang et al. (2020) illustrates that magnetospheric sawtooth oscillations can be solely induced by cusp O^+ outflows in the global simulation conducted by the LFM model.

The previous publications all show that the magnetotail reconnection is the key factor in inducing the sawtooth oscillations and the ionospheric outflow is affecting the reconnection rate. In this paper, we use the University of Michigan's Space Weather Modeling Framework (SWMF; Tóth et al., 2012) to investigate how kinetic reconnection affects the sawtooth oscillations under constant solar wind driving conditions. In addition to the global magnetohydrodynamics (MHD) model simulating Earth's magnetosphere, we are using the FLexible Exascale Kinetic Simulator (FLEKS) (Chen et al., 2021) in the magnetotail to model the tail reconnection with full kinetic physics. For comparison, we also present results by pure ideal MHD and Hall MHD models to emphasize the significance of the kinetic effects. Different from the previous work discussed above, we are not varying the plasma outflow from the ionosphere, hence the periodic oscillations observed are caused by the kinetic reconnection process embedded into the global MHD model.

The model description and simulation setup are described in Section 2, the simulation results are presented in Section 3 and we conclude in Section 4.

2. Model Description and Simulation Setup

The simulations presented in this paper are conducted with the magnetohydrodynamics with embedded particle-in-cell (MHD-EPIC) model (Chen & Tóth, 2019; Daldorff et al., 2014). The MHD-EPIC model two-way couples the BATS-R-US MHD code (Powell et al., 1999; Tóth et al., 2008) and the semi-implicit particle-in-cell code FLEKS (Chen et al., 2021) through the SWMF (Tóth et al., 2012). The global magnetosphere structure is simulated by an ideal MHD model, with an embedded PIC region in the magnetotail to simulate the kinetic physics in the magnetic reconnection. The ionospheric electrodynamics is simulated by the Ridley Ionosphere Model (RIM) (Ridley et al., 2004) that solves a Poisson-type equation for the electric potential on a 2-D spherical grid, which is used to set the $\mathbf{E} \times \mathbf{B}$ velocity at the inner boundary of BATS-R-US. The MHD-EPIC model has been applied in studying multiple planetary and moon magnetospheres, such as the Earth (Chen et al., 2017, 2020), Mars (Ma et al., 2018), Mercury (Chen et al., 2019), and Ganymede (Tóth et al., 2016; Zhou et al., 2019, 2020).

A three-dimensional block-adaptive Cartesian grid of BATS-R-US is used to cover the entire computational domain: $-224\ R_E < x < 32\ R_E$ and $-128\ R_E < y, z < 128\ R_E$ in GSM coordinates. The grid resolution is 1/4 R_E between $-60\ R_E < x < 20\ R_E$, $-20\ R_E < y < 20\ R_E$, and $-16\ R_E < z < 16\ R_E$. A shell region near the Earth from 2.5 R_E to 3.5 R_E is covered with 1/8 R_E grid resolution. The PIC box, the computational domain of FLEKS, is in the magnetotail between $-80\ R_E < x < -4\ R_E$, $-20\ R_E < y < 20\ R_E$, and $-10\ R_E < z < 10\ R_E$ with grid resolution 1/4 R_E. Figure 1 shows a 3-D overview of the simulation domain at $t = 3{,}600$ s from the simulation presented in this paper. The color contour is the mass density on the equatorial plane, and the magnetic field lines of two flux

ropes are also plotted in the magnetotail. The black box is the PIC domain, which covers the tail region where magnetic reconnection could happen.

To reduce the computational cost and make the simulation feasible, the speed of light c is reduced to 15,000 km/s to speed up the convergence of the implicit solver, and the ion-electron mass ratio m_i/m_e is decreased to 100 to increase the electron kinetic scales. These modification have no direct impact on the results at the ion and global scales. In addition to these numerical adjustments, we also scale up the ion and electron mass per charge by a factor of 16 to increase the ion inertial length so that it can be resolved with an affordable grid resolution. The ion inertial length in the magnetotail is larger than about 1 R_E with the scaling factor applied, which can be marginally resolved by the 1/4 R_E grid resolution. Tóth et al. (2017) presents theoretical arguments and numerical experiments and concludes that (a) the solution of the equations is not sensitive to the scaling at global scales and (b) the solution at the kinetic scale is proportional to the scaling factor but will look the same. The global scale features, including sawtooth oscillations, are not affected by the scaling factor.

The dipole tilt angle is set to 0° to form an idealized case. The inner boundary of BATS-R-US is at $r = 2.5\ R_E$, where the density is fixed at 28 amu/cc, the radial velocity is set to 0, and the tangential velocity is calculated from the ionospheric $\mathbf{E} \times \mathbf{B}$ drift. Floating (zero-gradient) boundary condition is set for temperature and the magnetic field $\mathbf{B}_1$ that is the difference between the total field and the dipole. This boundary condition does not prescribe ionospheric outflow, although plasma density is maintained at around 28 amu/cc and will be accelerated due to the external motional electric field in the open cusp region.

The solar wind condition applied at the inflow boundary of BATS-R-US is set to constant to study the magnetosphere's response to an idealized ICME solar wind driving. We have two solar wind conditions: (a) $V_x = -600$ km/s, IMF $B_z = -15$ nT for strong driving and (b) $V_x = -400$ km/s, IMF $B_z = -5$ nT for weak driving. The plasma number density and the temperature of the solar wind are fixed at 5 cm^{-3} and 10^5K, respectively. The solar wind velocity components V_y, V_z and IMF components B_x, B_y are all set to 0. Both strong and weak driving conditions are applied to the MHD-EPIC model to demonstrate that exceeding a threshold of the transported magnetic flux from the solar wind is necessary for triggering the sawtooth oscillation. We also run Hall MHD and ideal MHD models under strong driving to emphasize the importance of the kinetic reconnection. The Hall region, which covers the same simulation domain as the PIC region, is embedded in an ideal MHD simulation. We also apply the scaling factor 16 to the Hall MHD model. All three models are using the same grid in BATS-R-US.

We first run BATS-R-US and RIM for 15,000 steps using local time stepping with ideal MHD until the system reaches a quasi-steady state. Then the time accurate mode is turned on for 12 hr of physical time. The FLEKS model and/or the Hall MHD solver are switched on in the time accurate section.

3. Results

3.1. Occurrence of Sawtooth-Like Oscillations

A characteristic signature of sawtooth oscillations is the temporal variation of the magnetic inclination angle, which is defined as the angle $\alpha = \arcsin(|B_z|/B)$ between the magnetic field vector and the equatorial plane. Here, B_z and B are the local magnetic field Z component and magnitude, respectively. The change of the magnetic inclination angle results from the field line stretching and dipolarization processes. At the geostationary orbit, the average minimum inclination angle of an observed sawtooth is 26° as compared to 43° for the isolated substorms (Cai et al., 2006). Figure 2a shows the magnetic inclination angles observed at $r = 8\ R_E$ radial distance from the center of Earth, 9° latitude and 2 a.m. MLT. The corresponding GSM coordinates are $[x, y, z] = [-6.93, -4, 1.25]\ R_E$. Compared to the geostationary orbit, we are observing further toward the magnetotail because the variations detected at 6.6 R_E are small. Due to the $\pm Z$ symmetry, the inclination angle is 90° in the equatorial plane, so we extract values slightly above that plane. As we will see later, the largest variation of the inclination angle occurs slightly off from the midnight direction, this is why we chose 2 a.m. MLT.

The dashed gray line is the result of the ideal MHD model with strong solar wind driving, and the simulated magnetosphere takes about 2 hr to converge to a steady solution. There is no perturbation of the inclination angle, which stays at about 50° for the entire simulation. The solid gray line shows the result from the Hall MHD model with strong solar wind driving, which takes about 1.5 hr to reach a quasi-steady state. However, unlike the ideal MHD model, the inclination angle oscillates around 60° with a ±5° range. The difference in the average

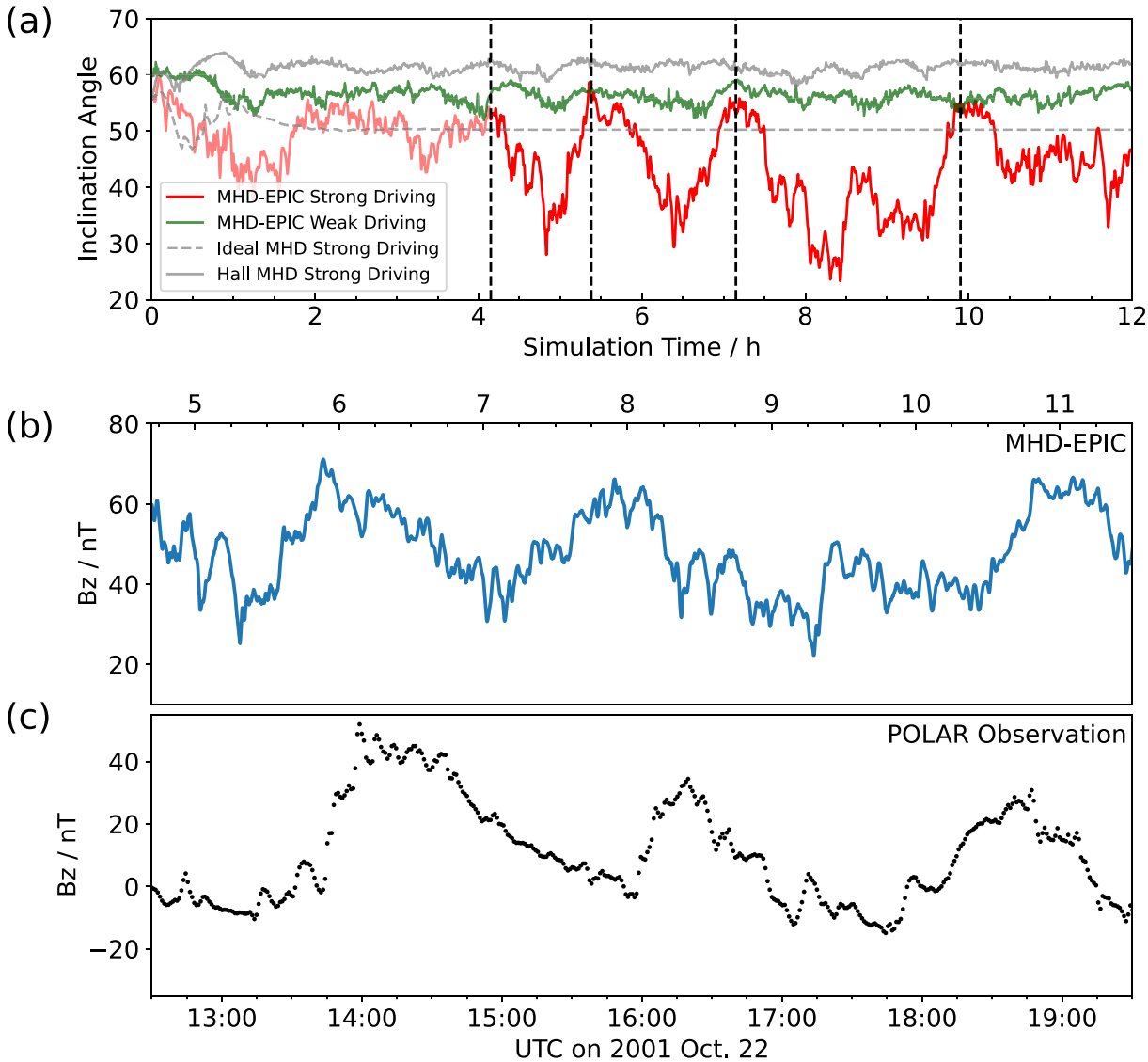

Figure 2. (a) Magnetic inclination angle plots from multiple simulations. Magnetohydrodynamics with embedded particle-in-cell (MHD-EPIC) with strong and weak solar wind driving conditions are shown in red and green. For comparison, the ideal and Hall MHD results under strong solar wind driving are also plotted in dashed and solid gray, respectively. All inclination angles are taken at the same position: $x = -6.93\ R_E$, $y = -4\ R_E$, and $z = 1.25\ R_E$. (b) Time variation of B_z at the same position from the MHD-EPIC simulation with strong driving. (c) Sawtooth event observations of B_z by the POLAR satellite from $(-8.0, 3.5, -2)\ R_E$ to $(-8.0, 3.5, 2)\ R_E$ in GSM coordinate (Figure 3 from Pulkkinen et al. (2006)).

inclination angles between the ideal MHD and Hall MHD models can be explained by the different reconnection modes resulting from the two models. Simulations show that the ideal MHD gives a Sweet-Parker type solution while the Hall MHD model gives a solution closer to the Petschek type (Murphy et al., 2009). Though they are different in the values of inclination angles, it is clear that there are no sawtooth-like oscillations in the ideal and Hall MHD simulation results.

The MHD-EPIC result with strong solar wind driving is shown by the solid red line, while the result of weak solar wind driving is plotted in green. The MHD-EPIC run with weak solar wind driving shows similar oscillation to the Hall MHD run, although with a smaller average inclination angle around 55°. The MHD-EPIC run with strong solar wind driving shows different inclination angle variations from the other three runs. After about 4 hr of the simulation, the inclination angle drops to about 30° from 55° with a recovering phase afterward. There are three sawteeth shown in Figure 2a and their starting times are marked by dashed vertical lines at $t = 4.15$, 5.38, and 7.15 hr. The third sawtooth shows a small dipolarization during the stretching phase. Partial dipolarizations

are consistent with observations as shown in the bottom panel of the figure. Panels (b) and (c) of Figure 2 compare the time variation of B_z from the MHD-EPIC simulation with strong solar wind driving and the observation from the POLAR satellite of the sawtooth event reported by Pulkkinen et al. (2006). The POLAR satellite trajectory is around $x = -8.0\ R_E$ and $y = 3.5\ R_E$ and moves from $-2\ R_E$ to $2\ R_E$ in GSM coordinate. The absolute values of B_z are different between the simulation and the observation because they are acquired at different positions, but the differences between the maximum and the minimum B_z for each sawtooth are around 40 nT in both. Furthermore, a partial dipolarization was observed by POLAR between 17:00 and 18:00 UT that is reminiscent of the simulation results between 9 and 10 hr.

From the four simulations with different setups presented in this section, we can conclude that two essential factors need to be satisfied for a global model to generate sawtooth-like oscillations without the time varying ionospheric outflow. First, the total eroded magnetic flux $\Phi_{MP} = \int_t v^{4/3} B_T^{2/3} \sin^{8/3}(\theta_c/2)\ dt$ needs to exceed a certain threshold, where t (s) is the duration of the stretching phase, v (m/s) is the solar wind velocity, $B_T\,[T]$ is the transverse field, and θ_c is the IMF clock angle. Cai and Clauer (2013) report a threshold value 10^6 Wb from multiple sawtooth events. The Φ_{MP} from the strong and weak solar wind conditions in our simulations are 3.1×10^5 and 1.1×10^6 Wb, respectively with an estimated value $t = 1$ hr. The observed threshold falls between these two solar wind conditions. Second, the tail reconnection needs to be simulated by the kinetic model.

3.2. Kinetic Reconnection and Sawtooth-Like Oscillations

In this subsection, we will investigate the connection between the sawtooth-like oscillations shown in Figure 2 and the kinetic reconnection process in the magnetotail. Panel (a) of Figure 3 shows the magnetic field, particle energy, and half of the total energy inside the PIC box normalized by the total energy at $t = 2$ hr. The electric field energy oscillates around 0.06% of the total energy, which is negligible compared to the energy of the magnetic field and the particles. The magnetic field and particles have a periodic energy gain/loss accompanied with the sawtooth oscillations.

Before $t = 4.4$ hr, there is no substantial energy transferred between the magnetic field and the particles. At $t \approx 4.4$ hr, the E_{magnetic} starts increasing while the E_{particle} starts decreasing. This stretching phase (S1) ends at $t \approx 5$h when the difference reaches about 10%. In the next dipolarization phase (D1) the energy is transferred back from the magnetic field to the particles. The two parts of energy recover to the initial state at $t \approx 5.4$ hr, which ends the first sawtooth period, and a similar oscillation starts at $t \approx 6$ hr and ends at $t \approx 7.5$ hr (S2 and D2). Panels (b)–(e) of Figure 3 depict the electron kinetic energy multiplied by the sign of the X component of the electron velocity that is defined as $K_e = \frac{1}{2}\rho_e u_e^2 \text{sgn}(u_{e,x})$. The K_e values are plotted on the $B_x = 0$ isosurface, which is the middle of the tail current sheet. We choose the electron kinetic energy because the electron features are well localized, and the sign change of K_e accurately indicates the position of the reconnection X line. The two blue vertical lines labeled S1 and S2 in panel (a) are marked at $t = 4$ hr 48 min and $t = 6$ hr 30 min when E_{magnetic} reaches the maximum in each period and their corresponding E_k contour plots are shown in panels (b) and (d). In these panels, the magnetosphere is in a "stretching phase," when the X lines move toward the distant tail at $x \approx -40\ R_E$. Another two red vertical lines labeled D1 and D2 in panel (a) are marked at $t = 5$ hr 14 min and $t = 7$ hr 01 min. Those two lines mark when E_{particle} (or E_{magnetic}) is increasing (or decreasing) most rapidly. Panels (c) and (e) show the corresponding E_k contour plots, when the magnetosphere is in a "dipolarization phase." In this phase, the X line is observed at $x \approx -15\ R_E$ and the E_k near the X line is much larger. The "dipolarization phase" is also matching the recovery from the minimum inclination angle observed in Figure 2. The third sawtooth oscillation in the simulation is more complicated than the previous two. The dipolarization phase is interrupted by a secondary stretching from $t \approx 8$ hr 36 min to $t \approx 9$ hr 24 min. The third oscillation fully recovers to the initial state at $t \approx 10$ hr. The period of the oscillations varies from 1.5 to 3 hr, which is very comparable with the observed periodicity.

3.3. Spatial Distribution of the Magnetic Inclination Angle

The wide extension of the variations of magnetic inclination angles in MLT is a critical signature of the sawtooth oscillations. Figure 4 shows the magnetic inclination contour plot from the MHD-EPIC simulation with strong solar wind driving conditions. The inclination angle is calculated along the circle $\sqrt{x^2 + y^2} = 7.9\ R_E$ in the plane $z = 1.26\ R_E$ (the inclination angle is 90° in the $z = 0$ plane due to the symmetry of this idealized setup). The

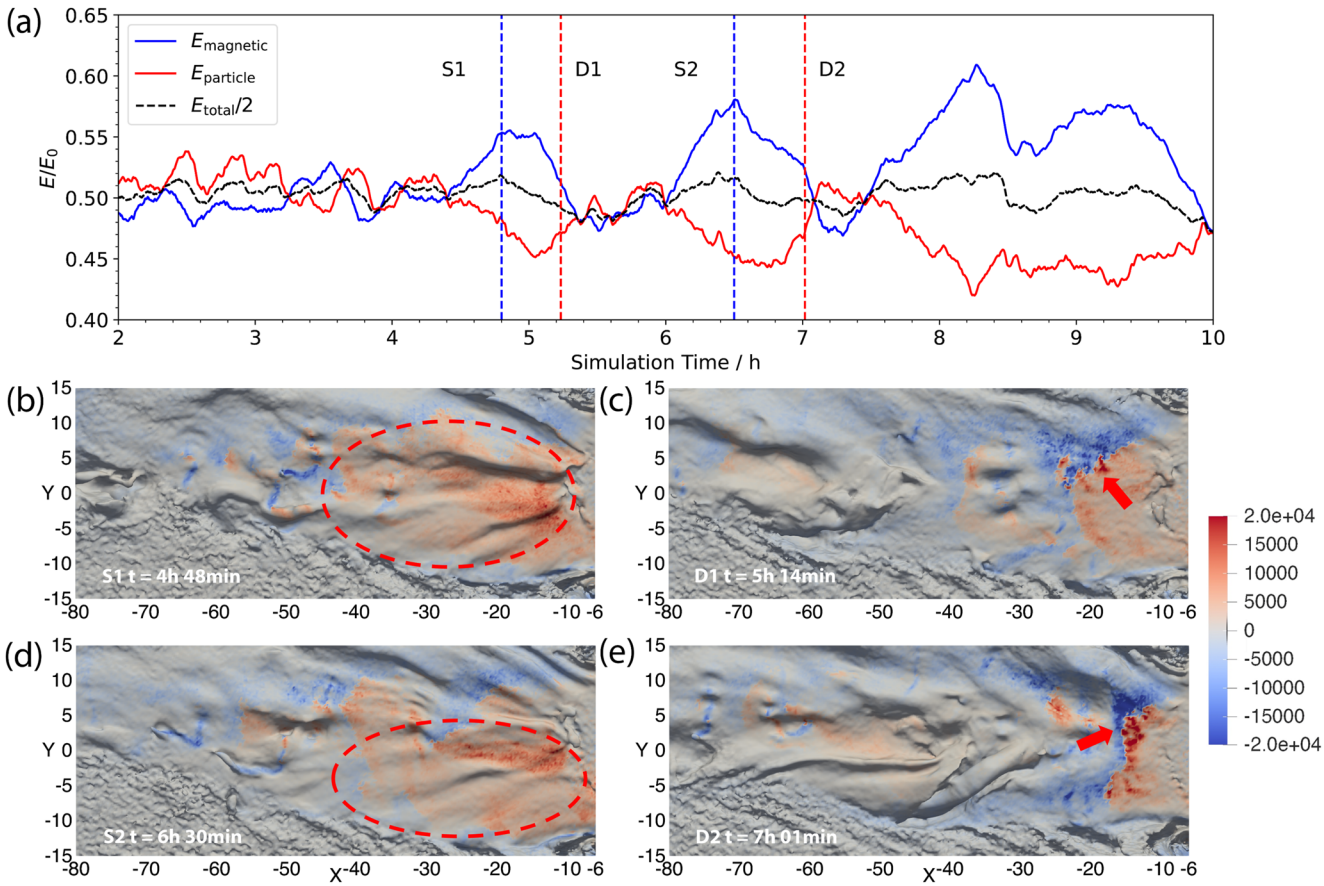

Figure 3. (a) The integrated magnetic field energy (blue) and particle energy (red) inside the PIC region normalized by the total energy at $t = 2$ hr. The black line shows half of the normalized total energy. The four dashed vertical lines correspond to the times depicted by panels (b–e), respectively, during the stretching (S1 and S2) and dipolarization (D1 and D2) phases. The stretching and dipolarization regions are highlighted by red circles and arrows, respectively. These plots show the color contours of the electron kinetic energy multiplied by the sign of the X component of the electron velocity: $K_e = \frac{1}{2}\rho_e u_e^2 \mathrm{sgn}(u_{e,x})$. The color contour is plotted on the $B_x = 0$ isosurface that identifies the middle of the magnetotail current sheet. Sharp jumps from dark blue to dark red color indicate reconnection jets emanating from the X-lines. The black shadows show that the current sheet surface is rippled.

location we are looking at is further from the center of Earth than the observations at the geosynchronous orbit reported by Cai et al. (2006). Our MHD-EPIC simulation does not produce strong magnetic field perturbations at geosynchronous orbit. Despite the difference in the locations, the simulated inclination angle distribution over MLT exhibits several similarities compared to the observations. The minimum inclination angle from dawn to dusk is about 17°, which is close to observed sawtooth oscillations. The broad span in MLT also agrees with the observation. The stretching and dipolarization phases with a period of around 1.5 hr are close to the observed periodicity.

While many features of the MHD-EPIC simulation results agree reasonably well with observations of sawtooth events (Cai et al., 2006), there are also several discrepancies. First, the signatures at the geosynchronous orbit are not strong enough to be observed, indicating that the stretching and dipolarization in the model are less energetic than in reality. Second, the stretching at midnight is much weaker than at dawn and dusk in the simulation. This is the reason why the inclination angle in Figure 2 is extracted at 2 a.m. MLT. The observed sawtooth oscillations exhibit the lowest inclination angle near midnight and expand toward dawn and dusk. Third, the duration of each sawtooth from the MHD-EPIC simulation varies from 1.5 to 3 hr, which is slightly shorter than a typically observed sawtooth that lasts from 2 to 4 hr.

One possible reason for the weaker signatures at midnight is that the "critical level" of the accumulated magnetic flux simulated by the MHD-EPIC model is lower than reality at dawn and dusk. The reconnection that happens

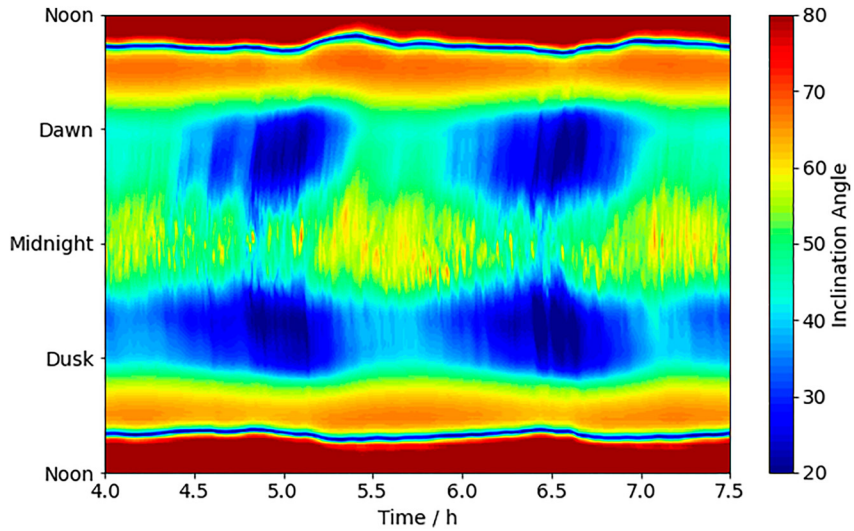

Figure 4. The contour plot of the magnetic inclination angle of the first two sawteeth from the magnetohydrodynamics with embedded particle-in-cell simulation with strong solar wind driving. The inclination angle is evaluated on the circle $\sqrt{x^2 + y^2} = 7.9\ R_E$ in the plane $z = 1.26\ R_E$, which is outside the geosynchronous orbit.

there first causes stronger dipolarization at dawn and dusk than observed, which dissipates the accumulated magnetic flux and preempts strong dipolarization at midnight.

4. Conclusion and Discussion

In this paper, we use the MHD with MHD-EPIC model to study the role kinetic reconnection plays in generating magnetospheric sawtooth events. The PIC region covers a box region in the magnetotail where the reconnection could potentially happen. Different from prior MHD simulations of sawtooth events, there is no time varying ionospheric outflow transporting plasma to the magnetotail. We apply both strong and weak solar wind driving conditions in the MHD-EPIC simulations to demonstrate that the occurrence of the sawtooth oscillations depends on the incoming rate of the magnetic flux from the solar wind. To emphasize the significance of the kinetic model, we also perform the simulation using ideal MHD and Hall MHD models with the strong solar wind driving conditions for comparison.

We examine the temporal variation of the magnetic inclination angle in the near tail at $(x, y, z) = (-6.93, -4, 1.25)\ R_E$ from different simulations. We find that only the MHD-EPIC model with strong solar wind driving condition produces periodic oscillations of the magnetic inclination angle that has a minimum value below 30°, which demonstrates that both the kinetic magnetic reconnection and the incoming rate of the magnetic flux from the solar wind are essential to induce the sawtooth oscillations. We investigate the variations of magnetic and particle energy from the MHD-EPIC simulation. The energy is transferred from the particles to the magnetic field during the stretching phase. When the dipolarization starts, the energy transfers in the opposite direction. We also plot the electron kinetic energy contour on the current sheet surface, and we observe that the dipolarization phase of the sawtooth oscillation is related to the formation of a reconnection X-line close to the Earth, which is consistent with observations (Henderson, 2004). We find that the oscillations from the MHD-EPIC simulation exhibit a wide span over the MLT that is a signature of observed sawtooth events. However, there are three major discrepancies between the MHD-EPIC generated sawtooth oscillations and the observations: (a) the signature at the geosynchronous orbit is relatively weak, (b) the simulated period of the sawtooth oscillations varies from 1.5 to 3 hr that is somewhat shorter than the observed periods of 2–4 hr, and (c) the minimum inclination angle in the simulation is found at the dawn and dusk regions rather than at midnight.

We suggest that the kinetic reconnection in the magnetotail can solely reproduce the periodic loading and unloading process of the magnetic flux in the magnetosphere. The kinetic model can accumulate the magnetic flux beyond a critical level on the nightside, which then triggers dipolarization. This process is recognized as the direct causing mechanism of the sawtooth oscillations (Zhang et al., 2020). However, the ideal and Hall MHD models

yield lower thresholds for dissipating the magnetic flux through numerical diffusion-driven reconnection. Thus those models cannot produce sawtooth-like oscillations. Hence we conclude that in addition to the ionospheric outflow, the sawtooth oscillations might be an intrinsic feature of the kinetic reconnection in the magnetotail when the incoming magnetic flux from the solar wind exceeds a threshold. However, the discrepancies between the observation and the MHD-EPIC simulation suggest that ionospheric outflow is also an important factor. The ionospheric O^+ transported into the magnetotail will change the plasma mass density and composition, which may make the stretching phase last longer. Also, the "preconditioning" by the nightside outflow mentioned by Zhang et al. (2020) might reduce the discrepancy at the midnight sector between the MHD-EPIC simulation and observations. In future work, we believe it is important to include both ionospheric outflow and kinetic magnetic reconnection physics in the magnetotail to fully understand sawtooth oscillations.

Data Availability Statement

The POLAR satellite data is obtained from the Coordinated Data Analysis Web (CDAWeb) from the NASA (https://cdaweb.gsfc.nasa.gov). The SWMF code (including BATS-R-US and FLEKS) is publicly available through the website (https://clasp.engin.umich.edu/research/theory-computational-methods/swmf-downloadable-software/) after registration. The simulation output and scripts used for generating figures in this paper can be obtained online (https://doi.org/10.7302/61te-2903) through the University of Michigan's Deep Blue Data repository, which is specifically designed for U-M researchers to share their research data and to ensure its long-term viability.

Acknowledgments
This work was primarily supported by the NSF PRE-EVENTS Grant No. 1663800. The authors acknowledge support from the NASA DRIVE Center at the University of Michigan under grant NASA 80NSSC20K0600. The authors acknowledge the Texas Advanced Computing Center (TACC) at The University of Texas at Austin for providing HPC and storage resources that have contributed to the research results reported within this paper.

References

Belian, R., Cayton, T., & Reeves, G. (1995). Quasi-periodic global substorm generated flux variations observed at geosynchronous orbit. *Space Plasmas: Coupling Between Small and Medium Scale Processes*, *86*, 143–148. https://doi.org/10.1029/gm086p0143

Brambles, O., Lotko, W., Zhang, B., Ouellette, J., Lyon, J., & Wiltberger, M. (2013). The effects of ionospheric outflow on ICME and SIR driven sawtooth events. *Journal of Geophysical Research: Space Physics*, *118*(10), 6026–6041. https://doi.org/10.1002/jgra.50522

Brambles, O., Lotko, W., Zhang, B., Wiltberger, M., Lyon, J., & Strangeway, R. (2011). Magnetosphere sawtooth oscillations induced by ionospheric outflow. *Science*, *332*(6034), 1183–1186. https://doi.org/10.1126/science.1202869

Cai, X., & Clauer, C. (2013). Magnetospheric sawtooth events during the solar cycle 23. *Journal of Geophysical Research: Space Physics*, *118*(10), 6378–6388. https://doi.org/10.1002/2013ja018819

Cai, X., Clauer, C., & Ridley, A. (2006). Statistical analysis of ionospheric potential patterns for isolated substorms and sawtooth events. *Annals of Geophysics*, *24*(7), 1977–1991. https://doi.org/10.5194/angeo-24-1977-2006

Chen, Y., & Tóth, G. (2019). Gauss's law satisfying energy-conserving semi-implicit particle-in-cell method. *Journal of Computational Physics*, *386*, 632–652. https://doi.org/10.1016/j.jcp.2019.02.032

Chen, Y., Tóth, G., Cassak, P., Jia, X., Gombosi, T. I., Slavin, J., et al. (2017). Global three-dimensional simulation of Earth's dayside reconnection using a two-way coupled magnetohydrodynamics with embedded particle-in-cell model: Initial results. *Journal of Geophysical Research: Space Physics*, *122*(10), 10318. https://doi.org/10.1002/2017JA024186

Chen, Y., Tóth, G., Hietala, H., Vines, S. K., Zou, Y., Nishimura, Y., et al. (2020). Magnetohydrodynamic with embedded particle-in-cell simulation of the geospace environment modeling dayside kinetic processes challenge event. *Earth and Space Science*, *7*(11), e2020EA001331. https://doi.org/10.1029/2020EA001331

Chen, Y., Tóth, G., Jia, X., Slavin, J. A., Sun, W., Markidis, S., et al. (2019). Studying dawn-dusk asymmetries of Mercury's magnetotail using MHD-EPIC simulations. *Journal of Geophysical Research: Space Physics*, *124*(11), 8954–8973. https://doi.org/10.1029/2019ja026840

Chen, Y., Toth, G., Zhou, H., & Wang, X. (2021). FLEKS: A flexible particle-in-cell code for multi-scale plasma simulations. *Earth and Space Science Open Archive*, 27. https://doi.org/10.1002/essoar.10508070.1

Daldorff, L. K. S., Tóth, G., Gombosi, T. I., Lapenta, G., Amaya, J., Markidis, S., & Brackbill, J. U. (2014). Two-way coupling of a global hall magnetohydrodynamics model with a local implicit particle-in-cell model. *Journal of Computational Physics*, *268*, 236–254. https://doi.org/10.1016/j.jcp.2014.03.009

Henderson, M. (2004). The May 2–3, 1986 CDAW-9C interval: A sawtooth event. *Geophysical Research Letters*, *31*(11), L11804. https://doi.org/10.1029/2004gl019941

Henderson, M., Reeves, G., Skoug, R., Thomsen, M., Denton, M. H., Mende, S., et al. (2006). Magnetospheric and auroral activity during the 18 April 2002 sawtooth event. *Journal of Geophysical Research*, *111*(A1), A01S90. https://doi.org/10.1029/2005ja011111

Henderson, M., Skoug, R., Donovan, E., Thomsen, M., Reeves, G., Denton, M. H., et al. (2006). Substorms during the 10–11 August 2000 sawtooth event. *Journal of Geophysical Research*, *111*(A6), A06206. https://doi.org/10.1029/2005ja011366

Huang, C.-S., Reeves, G., Borovsky, J., Skoug, R., Pu, Z., & Le, G. (2003). Periodic magnetospheric substorms and their relationship with solar wind variations. *Journal of Geophysical Research*, *108*(A6), 1255. https://doi.org/10.1029/2002ja009704

Lund, E. J., Nowrouzi, N., Kistler, L. M., Cai, X., & Frey, H. U. (2018). On the role of ionospheric ions in sawtooth events. *Journal of Geophysical Research: Space Physics*, *123*(1), 665–684. https://doi.org/10.1002/2017ja024378

Ma, Y., Russell, C. T., Toth, G., Chen, Y., Nagy, A. F., Harada, Y., et al. (2018). Reconnection in the Martian magnetotail: Hall-MHD with embedded particle-in-cell simulations. *Journal of Geophysical Research: Space Physics*, *123*(5), 3742–3763. https://doi.org/10.1029/2017ja024729

Murphy, N., Sovinec, C., & Cassak, P. (2009). Simulation and analysis of magnetic reconnection in an experimental geometry. In *Bulletin of the American Astronomical Society* (Vol. *41*, p. 514).

Ouellette, J., Brambles, O., Lyon, J., Lotko, W., & Rogers, B. (2013). Properties of outflow-driven sawtooth substorms. *Journal of Geophysical Research: Space Physics*, *118*(6), 3223–3232. https://doi.org/10.1002/jgra.50309

Powell, K., Roe, P., Linde, T., Gombosi, T., & De Zeeuw, D. L. (1999). A solution-adaptive upwind scheme for ideal magnetohydrodynamics. *Journal of Computational Physics*, *154*(2), 284–309. https://doi.org/10.1006/jcph.1999.6299

Pulkkinen, T., Ganushkina, N. Y., Tanskanen, E., Kubyshkina, M., Reeves, G., Thomsen, M., et al. (2006). Magnetospheric current systems during stormtime sawtooth events. *Journal of Geophysical Research*, *111*(A11), A11S17. https://doi.org/10.1029/2006ja011627

Ridley, A., Gombosi, T., & Dezeeuw, D. (2004). Ionospheric control of the magnetosphere: Conductance. *Annales Geophysicae*, *22*(2), 567–584. https://doi.org/10.5194/angeo-22-567-2004

Tóth, G., Chen, Y., Gombosi, T. I., Cassak, P., Markidis, S., & Peng, B. (2017). Scaling the ion inertial length and its implications for modeling reconnection in global simulations. *Journal of Geophysical Research: Space Physics*, *122*(10), 10336. https://doi.org/10.1002/2017JA024189

Tóth, G., Jia, X., Markidis, S., Peng, B., Chen, Y., Daldorff, L., et al. (2016). Extended magnetohydrodynamics with embedded particle-in-cell simulation of Ganymede's magnetosphere. *Journal of Geophysical Research: Space Physics*, *121*(2), 1273–1293. https://doi.org/10.1002/2015JA021997

Tóth, G., Ma, Y. J., & Gombosi, T. I. (2008). Hall magnetohydrodynamics on block adaptive grids. *Journal of Computational Physics*, *227*(14), 6967–6984. https://doi.org/10.1016/j.jcp.2008.04.010

Tóth, G., van der Holst, B., Sokolov, I. V., Zeeuw, D. L. D., Gombosi, T. I., Fang, F., et al. (2012). Adaptive numerical algorithms in space weather modeling. *Journal of Computational Physics*, *231*(3), 870–903. https://doi.org/10.1016/j.jcp.2011.02.006

Wiltberger, M., Lotko, W., Lyon, J. G., Damiano, P., & Merkin, V. (2010). Influence of cusp O^+ outflow on magnetotail dynamics in a multifluid MHD model of the magnetosphere. *Journal of Geophysical Research*, *115*(A10), 148–227. https://doi.org/10.1029/2010JA015579

Yu, Y., & Ridley, A. J. (2013). Exploring the influence of ionospheric O^+ outflow on magnetospheric dynamics: Dependence on the source location. *Journal of Geophysical Research: Space Physics*, *118*(4), 1711–1722. https://doi.org/10.1029/2012ja018411

Zhang, B., Brambles, O. J., Lotko, W., & Lyon, J. G. (2020). Is nightside outflow required to induce magnetospheric sawtooth oscillations. *Geophysical Research Letters*, *47*(6), e2019GL086419. https://doi.org/10.1029/2019gl086419

Zhou, H., Tóth, G., Jia, X., & Chen, Y. (2020). Reconnection-driven dynamics at Ganymede's upstream magnetosphere: 3-D global Hall MHD and MHD-EPIC simulations. *Journal of Geophysical Research: Space Physics*, *125*(8), e2020JA028162. https://doi.org/10.1029/2020ja028162

Zhou, H., Tóth, G., Jia, X., Chen, Y., & Markidis, S. (2019). Embedded kinetic simulation of Ganymede's magnetosphere: Improvements and inferences. *Journal of Geophysical Research: Space Physics*, *124*(7), 5441–5460. https://doi.org/10.1029/2019ja026643